PCCP

Accepted Manuscript

ROYAL SOCIETY OF CHEMISTRY

rsc.li/pccp

View Article Online
DOI: 10.1039/C7CP07274K

ARTICLE Journal Name

Conformational switching via intramolecular H-bond modulates fluorescence lifetime in a novel coumarin-imidazole conjugate

Received 00th January 20xx,
Accepted 00th January 20xx

DOI: 10.1039/x0xx00000x

www.rsc.org/

Indranil Bhattacharjee[a], Nita Ghosh[b], Abhinav Raina,[a] Jyotishman Dasgupta[b] and Debdas Ray*[a]

Achieving synthetic control on light-driven molecular dynamics is essential for designing complex molecule-based devices. Here we design a novel coumarin-imidazole conjugate **1** whose excited state structural dynamics is primarily controlled by a distant intramolecular H-bonding interaction within the backbone. The coumarin conjugate is based on 1,2,4,5-aryl substituted imidazole framework (aryl = −Ph and −PhOH) covalently connected to the coumarin moiety via a C–N bond. A carefully positioned OH group in the aryl part of the imidazole fragment resulted in achieving two dissimilar O–H•••N and O–H•••O distal intramolecular hydrogen bonding interactions. NMR studies in conjunction with density functional theory (DFT) at the B3LYP/6-311G(d,p) level of theory shows the existence of two ground state conformers with rotational barrier of 6.12 kcal.mol^{-1}. Due to the presence of conformational isomers of **1**, the local excited state dynamics of the parent coumarin gets biased towards a long-lived fluorescent state with diminished non-radiative decay channels. Time-resolved emission studies show a *ca*. 4-5 times increase in the excited state lifetime in **1** when compared to coumarin-imidazole conjugate, **2** and **3**, without OH group. Solvent dependent studies show that, effect of solvent polarity, H-bonding donating ability and viscosity dictate the conformational distribution in the ground state as well as the dynamical evolution to the final emissive state. Our studies highlight the importance of rotamerism around C1–C4 single bond which leads to rigidification along courmarin-imidazole backbone through a combination of distal H-bonding and solvent interactions. The concept of new emission signaling pathways caused by conformational switching between two states offers a new paradigm to introduce functional allostery in macromolecular backbones.

Introduction

Radiative pathways in photoactive chromophores can be tuned by introducing rigidity of the molecular backbone through either covalent or non-covalent interactions.[1-5] Such tailoring of chemical interactions provides opportunities to optimize the optoelectronic properties inherent to the electronic structure of a fluorophore.[6-21] An increasing number of sensory systems have now been built on this principle, in which conformational change along the molecular backbone is tightly coupled to changes in the optical or electrochemical signal output.[22-35] Continuing challenges in such efforts lie in the invention of novel molecular systems in which fluorescence signalling pathway is controlled via conformational switching.

Here we describe the synthesis of a new series of coumarin-imidazole conjugates having tunable emission lifetimes dictated by a carefully positioned –OH group in the phenyl attached to C1 atom of the imidazolyl ring. Our design feature is highlighted in molecule **1** (Scheme 1) which is constructed by conjugating 1,2,4,5-aryl substituted imidazole (aryl = –Ph and –PhOH) with 7-diethylaminocoumarin moiety via a C–N bond. The exciting possibility of stabilizing two dissimilar O–H•••N and O–H•••O distal intramolecular hydrogen bonding (H-B) interactions in the same framework is tested by synthesizing the corresponding functional group substituents (–OCH_3, **2** and –H, **3**) at the –OH position. Due to the presence of these dissimilar H-bonds **1** may lead to conformational isomers (syn/anti)[36-44] caused by rotamerism around the C1–C4 single bond rotation. NMR studies in conjunction with density functional theory (DFT) at the B3LYP/6-311G(d,p) level show a distinct conformational distribution in the ground state. Fluorescence upconversion along with time resolved emission studies ensure that the excited state dynamics of the parent coumarin gets biased towards a long-lived fluorescent state with diminished non-radiative decay channels in **1**, when compared to coumarin-conjugate **2** and **3** (Scheme 2), without OH group. The distal intramolecular H-bond leads to rigidification along coumarin-imidazole backbone.

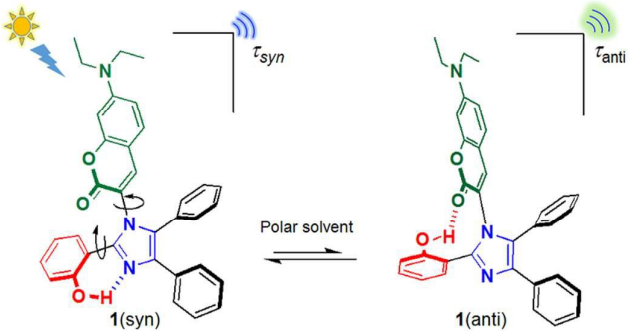

Scheme 1 Conformational changes of **1** through distal H-bond.

Synthesis and Characterization

The synthesis of **1** was achieved in three steps (Scheme 2). First, 4-diethylaminosalicyaldehyde is treated with ethyl nitroacetate to obtain **1a**.[45] Reduction ($SnCl_2$) of **1a** in water

[a] *Department of Chemistry, School of Natural Sciences, NH-91, Tehsil Dadri, District Gautam Buddha Nagar, Uttar Pradesh, 201314, India.*
[b] *Department of Chemical Sciences, Tata Institute of Fundamental Research, B-127, Mumbai-1, Homi Bhabha Road, 400005, India.*

†Electronic Supplementary Information (ESI) available: CCDC 1567243 and 1567244. For ESI and crystallographic data in CIF or other electronic format see DOI: 10.1039/x0xx00000x

View Article Online
DOI: 10.1039/C7CP07274K

followed by multicomponent condensation reaction[46] with salicyalaldehyde, benzil and ammonium acetate, purification by column chromatography (SiO_2, hexanes/toluene, 7:3, respectively) gives **1** in 55% isolated yield as yellow powder. Similarly, two controlled compounds, **2** and **3** were synthesized following the above protocol to yield **2** (62%) and **3** (70%) as yellow powder. All compounds were characterized by 1H and 13C NMR spectroscopies, high-resolution mass spectrometry, MALDI-TOF and X-ray crystallography (in the ESI†).

X-ray crystal structures

Crystals of **1** suitable for X-ray analysis were obtained from a slow evaporation of toluene solution resulted in the rectangular shaped yellow crystals. A similar procedure resulted in the cubic shaped yellow crystals of second reference compound, **3**.[47] The crystal structure determination data are tabulated in Table S1†, and selected bond lengths and bond angles are summarized in Table S2.† Single crystallographic analysis (Fig. 1a) of **1** reveals that there is an intramolecular H-bond (O–H•••N, 1.895 Å, 147.3°) between the imidazolyl nitrogen (N1) and the OH proton, which confirms syn configuration in the solid state. The measured dihedral angles indicate that the phenyl, coumarin and imidazolyl rings deviate from planarity 67.2(4)° (phenyl ring attached to C2), 6.6(5)° (phenyl ring attached to C3) and -92.1(4)° (coumarin ring attached to N2) when viewed along the N(2)–C(2)–C(19)–C(20), N(1)–C(3)–C(30)–C(29) and the C(2)–N(2)–C(10)–C(12) atoms, respectively. More importantly, the analysis shows that the measured torsion angle in **1** when viewed along the N(1)–C(1)–C(4)–C(5) atoms is 24.5(4)° which is almost *ca.* 25 times bigger compared to those of similar intramolecularly hydrogen-bonded imidazole derivatives[48-50], indicating that the hydroxyphenyl group in **1** significantly deviates from planarity resulting in a weaker H-bond. For comparison, the corresponding torsion angles of reference compound **3** (Fig. 1b, and Fig. S20†) are 76.1(3)°, 21.9(3)°, -83.3(3)°, and -27.0(3)° respectively. It is clear that orientation of the phenyl and coumarin moieties attached to C1, C2, C3 and N2 atoms of imidazolyl ring are significantly affected due to absence of the intramolecular hydrogen bonding interaction. Further, the crystal structure of **1** indicates that the O1 atom from coumarin group is hydrogen bonded with atom H12 of adjacent coumarin ring (C12–H•••O1, 2.381 Å, 153.63°). Moreover, an intermolecular C–H•••C interaction between atoms C5 and H23 (C23–H23•••C5, 2.9 Å, 126.71°), respectively is also present in the crystal lattice. In addition to this, a head to head π-π stacking (3.748 Å) interaction between –PhOH groups of neighbouring molecules is also seen. Thus, **1**

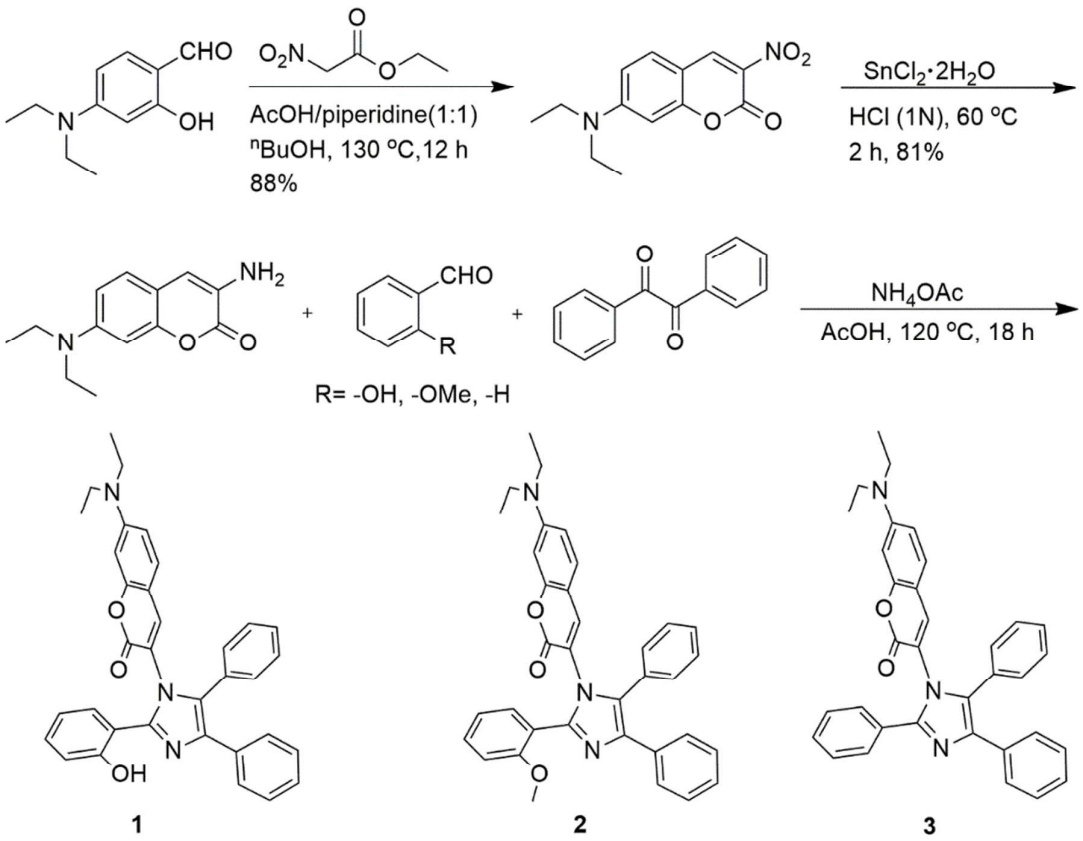

Scheme 2 Synthetic scheme and chemical structure of **1**, **2**, and **3**.

View Article Online
DOI: 10.1039/C7CP07274K

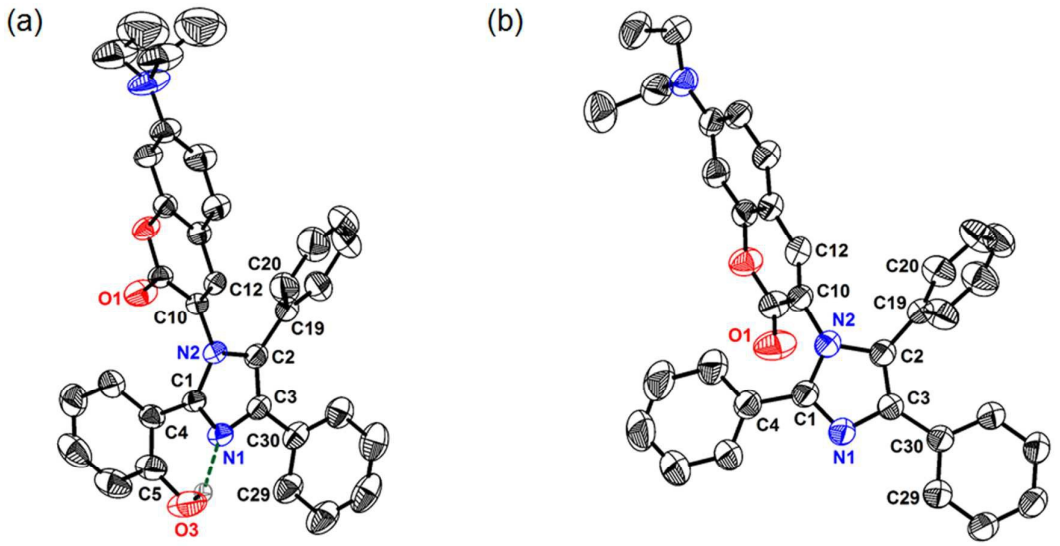

Fig. 1 Oak Ridge thermal ellipsoid plots (50% probability ellipsoids) of the X-ray structures of (a) **1** and (b) **3**. The hydrogens except OH are omitted for clarity.

crystallizes into cylindrical structure through head to head π-π stacking (3.753 Å), as seen along the b-axis (Fig. S19†). The crystals of **3** shows two intermolecular hydrogen bond between atoms of N1 and H20 from two neighbouring molecules (C20−H20•••N1, 2.656 Å, 145.9°) and atoms of O1 and H31 (C31−H31B•••O1, 2.347 Å, 143.1°). Moreover, two C−H•••C interactions between atoms of C26 and H9 (C9−H9•••C26, 2.891 Å, 132.6°) and C14 and H7 of two adjacent molecules (C7−H7•••C14, 2.835 Å, 160.26°), respectively are also present in the crystal lattice. Thus, **3** prefers to pack in head to tail fashion, as viewed along a-axis (Fig. S20†).

Steady State Absorption and Emission

All the synthesized compounds **1**, **2** and **3** were completely characterized by steady-state absorption spectroscopy (Fig. 2). For comparison, steady state absorption spectra of **1** and **2** are measured in solvents of different polarity (Table 1). The absorption feature peaked at ca. 400 nm is assigned to the coumarin absorption[51] and it arises from the charge transfer (CT) transition within the coumarin fragment.[51] For **1**, λ_{max} of the absorption bands located at ca. 373, 391, 395, and 403 nm, respectively, ongoing from nonpolar to polar solvents (cyclohexane (CHx), ACN, EtOH, ethyleneglycol (EtGly)), are shifted bathochromically. Likewise, for compound **2**, similar trend was noticed. The intramolecular charge transfer character of the absorption bands[52-56] was further supported by the observation of blue shift in non-polar solvent cyclohexane (CHx). Following the same line of thought, steady state emission measurements were also done in solvents having disparate polarity. Emission spectra of both **1** and **2** (λ_{ex} = 400 nm) show broadband features with positive solvatochromism effects (Fig. 2), leading to moderate Stoke's shifts of ca. 31-80 nm. This Stoke's shift leads us to conclude that both **1** and **2** are less polar in the Franck-Condon (FC) region compared to S1 minimum from which the emission occurs.[57] The excitation spectrum of **1** recorded in cyclohexane is independent of λ_{ex} and overlaps exactly with (Fig. S21a†) the absorption, which indicates the presence of a single species in ground state in cyclohexane solution. However, excitation spectra of **1** in polar solvents become dependent on λ_{em} and does not exactly overlap with absorption spectra (Fig. S21b†), indicating its origin from the presence of either an impurity or more than one coexisting ground-state conformers. Since, purity of thee samples was confirmed by NMR and crystallization, we eliminate the presence of any impurity, thereby assigning the observed features due to possibility of co-existing ground state conformers.

Time correlated single photon counting (TCSPC)

Time-correlated single-photon counting (TCSPC) (see experimental section for details) was used to monitor the excited state lifetimes of **1**, **2**, and **3** in solvents of varying polarity. Solvent dependent behaviour of coumarin dyes is well studied in the literature.[20,21,57,58] However, lifetime of coumarin emissive state can be modulated by other dominant non-radiative pathways. From our measurements, we find out that compounds **2** and **3** have radiative lifetimes ranging from *ca*. 400 ps to 1.29 ns, which is distinctively shorter than the parent coumarin chromophore having a fluorescence lifetime of ca. 3-5 ns (Table 1). These values indicate that non-radiative decay channels dominate the excited state lifetime of imidazole-coumarin conjugates **2** and **3**. On the contrary, for compound **1,** which has a carefully designed –OH substitution, the lifetime in all the solvents is 4 to 5 times longer than its –OCH_3 and –H counterparts. Additionally steady state emission

View Article Online
DOI: 10.1039/C7CP07274K

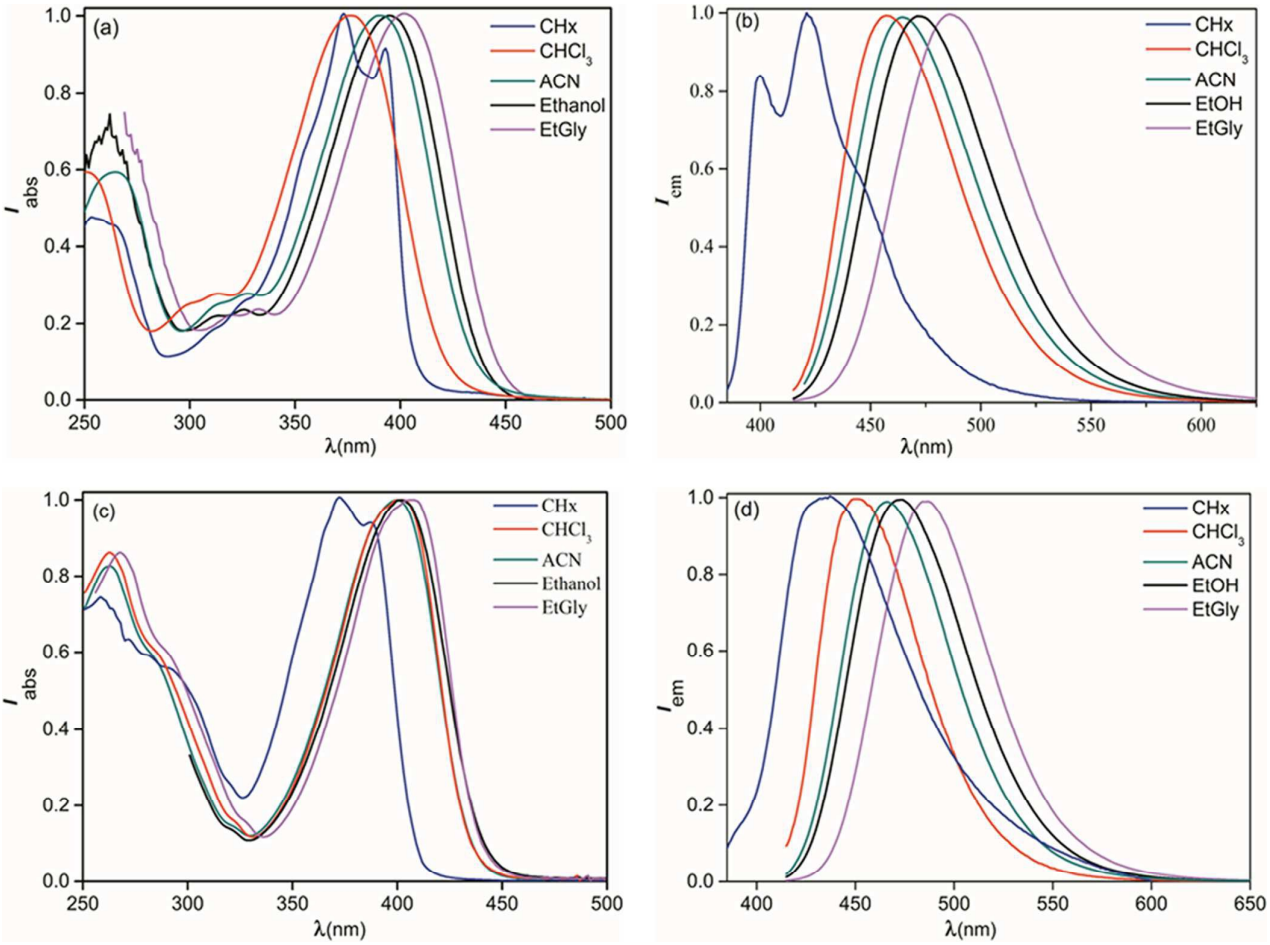

Fig. 2 UV/vis and steady state emission spectra (a, b) of **1**, and (c, d) of **2**. All spectra were recorded in various solvents at 298 K. Solvents are highlighted in color: CHx, blue; ACN, Dark Cyan; EtOH, Black; $CHCl_3$, Red; EtGly, Magenta.

spectra of **1** is highly broader than that of the other two substituents. To confirm the origin of the broadened red-edge, we collected time-resolved emission data at 538 nm along with data recorded at 475 nm, close to the peak maximum of the emission observed in all the three compounds. Fig. 3 and Fig. S25-S26† show the emission dynamics of all three compounds at 475 nm. The long-lived emission from an intramolecular charge-transfer coumarin excited state at 475

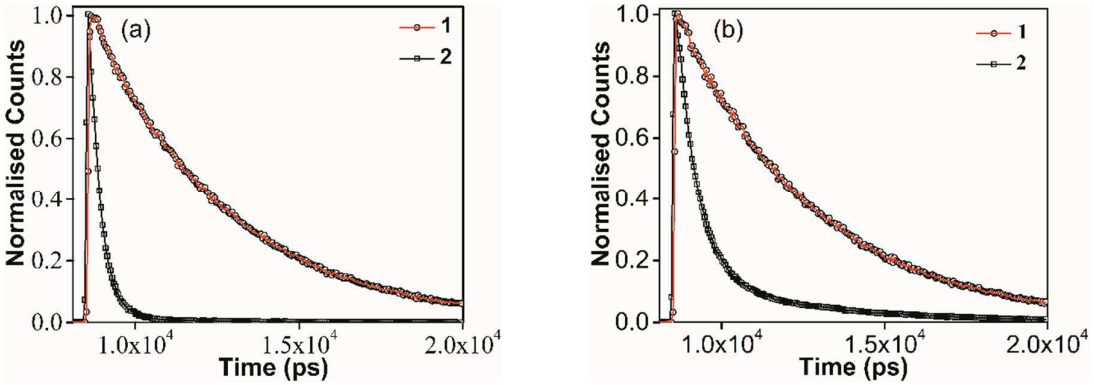

Fig.3 TCSPC decay profile of **1** and **2** in **a**) EtOH (λ_{em} = 475 nm), b) EtGly (λ_{em} = 475 nm).

View Article Online
DOI: 10.1039/C7CP07274K

Table 1 Steady state photophysical data of **1** and **2**.

Solvent (E_T(30))	λ_{abs} (nm)	ε (L mol^{-1} cm^{-1})	λ_{em} (nm)	$\Delta\nu$ (nm)	ϕ_f (%)	τ (ns) λ_{475} (nm)	τ (ns) λ_{538} (nm)
			1				
CH (31.2)	373, 393	3.0×10^4	404, 420[b]	31	78.8	-	-
MeCN (46.0)	391	4.6×10^4	464[a]	73	82.5	3.19	3.56
EtOH (51.9)	395	1.0×10^5	472[a]	77	88.1	4.0	4.08
EtGly (53.8)	403	3.0×10^4	485[a]	82	91.5	4.11	4.23
			2				
CH (31.2)	372, 387	1.1×10^4	425[b]	58	18.1	-	-
MeCN (46.0)	400	3.5×10^4	473[a]	74	20.6	0.73	0.76
EtOH (51.9)	402	3.6×10^4	465[a]	63	23.9	0.37	0.42
EtGly (53.8)	411	1.1×10^4	486[a]	75	26.4	0.99	1.19

[a]excitation wavelength (λ_{ex}) 400 nm, [b]excitation wavelength (λ_{ex}) 375 nm

nm in **1** implies a mechanism by which non-radiative decay channels have been slowed down. One possibility could be that the distal intramolecular H-bonding in **1** leads to rigidification of the coumarin unit thereby diminishing non-radiative decay channels. Since we detected a red-shifted emission at 538 nm with similar lifetimes, we suggest that a new radiative decay path which is a subtle function of molecular structure and viscosity, dictates the photophysics.

Quantum yield

Fluorescence quantum yields (ϕ_f) in different solvents were determined by comparing the spectrum with that of standard Fluorescin[59-60] (ϕ_f = 0.85 in 0.1(N) NaOH) taking total area under the emission spectra. It is noteworthy that, a significant variation in the quantum yield of **1** and **2** (Table 1), were observed. Compound **2** shows lower ϕ_f, while **1** shows remarkably high quantum yield in all solvents, which indicates that the intramolecular H-bond (O–H•••N) between OH proton and nitrogen atom of imidazolyl ring plays a crucial role to maintain structural rigidity of **1**. Interestingly, measured ϕ_f value of **1** further increases on going from non-polar to polar and viscous solvents (cyclohexane, CH_3CN, EtOH, ethyleneglycol (EtGly). These results suggest that a severe structural re-adjustment of **1** might be established by distal intramolecular H-bond (O–H•••O) between OH proton and keto carbonyl group of coumarin segment in the excited state. In contrast to **1**, the ϕ_f of **2** are also increased with solvent polarity, which ensures pronounced intramolecular charge transfer (ICT)[58] and reduced rotational motion associated with the backbone. Thus, increased ϕ_f of **1** in solvents of different polarity results from the combination of structural rigidity caused by intramolecular distal H-bond and ICT. These results are also consistent with the TCSPC measurements which show a *ca*. 4-5 times enhancement in the lifetime of the excited state.

Upconversion measurement

To gain a detailed understanding of the emission dynamics on an ultrafast timescale for **1**, fluorescence upconversion measurements[61] (see experimental section for details) were performed. To correlate with steady state emission spectra, upconversion decays were collected at two wavelengths, 475 nm and 538 nm upon selective coumarin excitation at 400 nm. Transients were fit with four exponential decay function convoluted with an instrument response function of 250 fs. Relevant fitting parameters are summarized in Table 2. Fig. 4 and S23† shows fluorescence upconversion transients of **1** and **2**, respectively in solvents of different polarity. Furthermore, the decay kinetics of this state measured in polar aprotic solvents indicate a clear polarity dependence of lifetime. However, in polar protic solvents, we see a rise time. The rise time further increases in ethylene glycol which indicates viscosity dependence to the evolution to this state. It is clear from the time-resolved emission data that viscosity and proton accepting ability of the solvent lead to two opposite effects, thereby playing critical role in determining the excited state evolution pathways for **1.** The dependence of excited state dynamics on protic solvent can be explained by the possibility of distal intramolecular H-bonding in **1**. In this framework, the upconversion transients suggest that decay at 475 nm channel is associated with extension of conjugation along coumarin backbone which is directed by an intramolecular H-bond between OH proton of hydroxyphenyl group and N1 atom of imidazolyl ring. Our conjecture is that this process is preceded by a rotation around C1–C4 single bond on the conjugate. The timescale for this geometrical re-adjustment suggests emission from locally excited state. Previous line of arguments for emission channel at 475 nm also holds true for emission collected at 538 nm. Moreover, we observed rise time of *ca*. 26 ps measured in ethylene glycol (Table 2) that is significantly higher when compared with ethanol. This observation clearly suggests that emission in this channel is originating from a state of completely new characteristics that follows a rotational reaction coordinate. This geometric re-adjustment might be assisted with torsion along with atoms of N1–C1–C4–C5 introducing increased planarity along the backbone. On the other hand, **2** shows, almost similar

View Article Online
DOI: 10.1039/C7CP07274K

Table 2 Fluorescence upconversion data of **1** and **2**.

Solvent	λ_{475} (nm)			λ_{538} (nm)		
	τ_1(ps)	τ_2(ps)	τ_3(ps)	τ_1(ps)	τ_2(ps)	τ_3(ps)
			1			
MeCN	-	22.4 ± 0.8	1669.4 ± 120	0.4 ± 0.1 (rise)	20.82 ± 1.16 (0.54)	5000 ± 0 (0.46)
EtOH	1.2 ± 0.5 (rise)	129.77 ± 31.6 (0.26)	1837.9 ± 0 (0.74)	0.7 ± 0.1 (rise) (0.54)	147.8 ± 1.8 (rise) (0.46)	4584.1 ± 0
EtGly	0.8 ± 0.2 (rise)	48.9 ± 2.8 (0.25)	2173.9 ± 0 (0.75)	2.7 ± 0.7 (rise) (0.32)	26.2 ± 3.6 (rise) (0.68)	4187.4 ± 0
			2			
MeCN	2.01± 0.1	14.7 ± 0.4	275.5 ± 13.4	4.9 ± 0.2	75.36 ± 2.95	-
EtOH	5.4 ± 0.1	105.2 ± 2	1806.2 ± 320	5.4 ± 0.6	202.7 ± 0	-
EtGly	5.1 ± 0.5	66.3 ± 3.5	1025.4 ± 98.4	-	-	482.1 ± 0

[a]excitation at 400 nm, and emission at 475 nm and 538 nm, respectively.

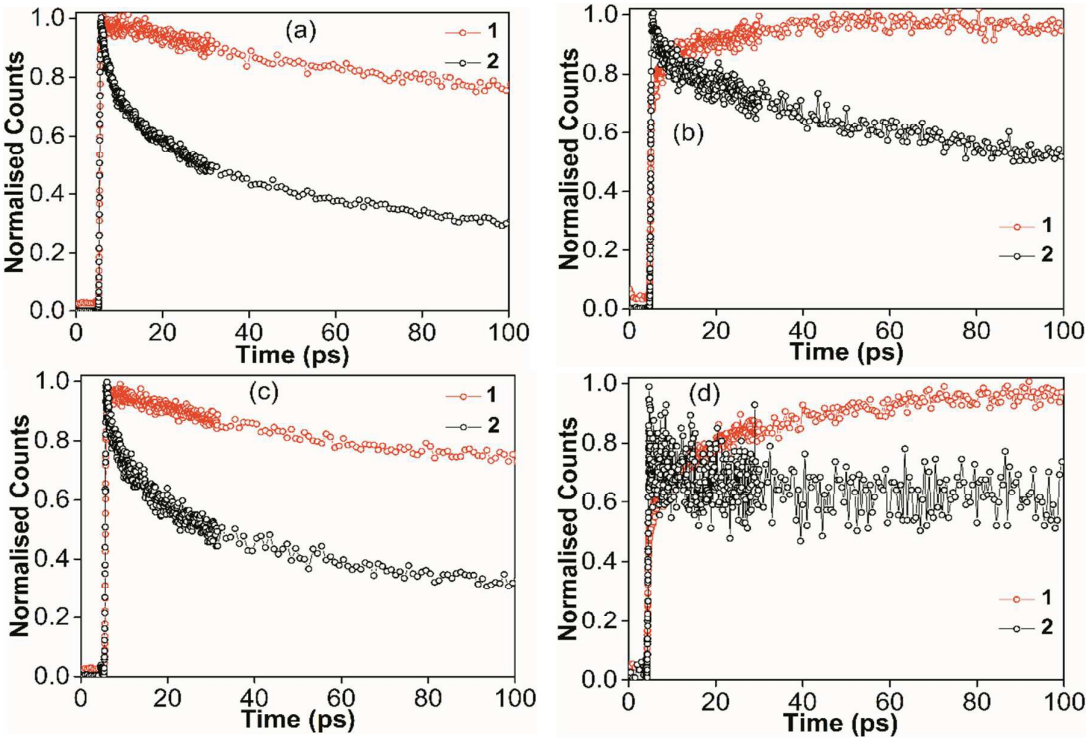

Fig. 4 Upconversion decay profile of **1** and **2** in a) EtOH (λ_{em} = 475 nm), b) EtOH (λ_{em} = 538 nm), c) EtGly (λ_{em} = 475 nm), and d) (λ_{em} = 538 nm). λ_{ex} = 400 nm.

decay kinetics, which indicates that emission at 475 and 538 nm, respectively have same origin. The decay kinetics were also comparable to the decay transients at 475 nm (Table 2 and Fig. 4) which further ensure that emission at these channels are coming from a single emissive state of **2**. Evaluation to this state involves rotational motion along the backbone, indicating more sterically hindered motion. However, for **1**, other than the decay kinetics being different, the effect of viscosity and protic dependence are much pronounced compared to emission at 475 nm channel, indicating geometrical re-adjustment along the line of proton transfer reaction co-ordinate which might be the limiting factor towards evolution to this new emissive state. It should be noted that no difference in the excited state dynamics of **3** (Fig. S24†) is observed compared to **2**, indicating OH chromophore of the phenyl group attached to C1 atom of

View Article Online
DOI: 10.1039/C7CP07274K

imidazolyl ring plays a dominant role for such intriguing geometrical re-adjustment. This further substantiate our observation in the TCSPC measurements.

NMR Analysis

The ground state conformational heterogeneity of molecule **1** was proved using a combination of both 1D and 2D-NMR spectroscopy along with temperature dependent spectral changes. The ^{1}H NMR spectrum of **1** in $CDCl_3$ shows a broad signal at 13.26 ppm (Fig. 5a), indicating presence of an exchangeable proton. In CD_3CN, however, we observe two distinct peaks at 13.08 and 8.12 ppm assigned to –OH protons (Fig. 5b). Since –OH protons are ionizable, the sample in CD_3CN was mixed with small amount of D_2O (30:1 v/v) to confirm exchange of the ionizable protons with deuterons. As shown in Fig. 5c, peaks at 8.12 and 13.08 ppm in CD_3CN as well as 13.26 ppm in $CDCl_3$ disappeared confirming our assignment of –OH group in the conjugate. The observation of an additional OH proton peak at 8.12 in CD_3CN indicates the presence of another conformer in solution. The aromatic peaks that appear at 6.55, 6.68, 7.02, 7.81, and 8.49 ppm in the ^{1}H NMR spectrum recorded in CD_3CN at RT (Fig. 5b) were difficult to assign due to dynamic equilibrium between the conformers. Therefore, ^{1}H NMR along with NOESY measurements were carried out at 273 K. We find NOESY correlation in the 1D-NOESY spectrum between proton H29 from the phenyl attached to C3 atom of imidazolyl ring and -OH proton at 13.08 ppm thereby confirming that $\mathbf{1}_{syn}$ conformation is one of the molecular geometries in solution at 273 K (Fig. S14a†). We confirm that the peak appeared at 7.81 corresponds to H12 proton of coumarin unit, as this signal shows a typical NOESY correlation (Fig. S14b†) with the H14 proton signal at 6.55 ppm. We come to the same conclusion when we compare a correlation spectroscopy (COSY) interaction between proton at 6.68 (H15) and 6.55 (H14) ppm (Fig. S13†). Similarly, the peak appeared at 7.02 ppm corresponds to H17 proton of coumarin unit, as this signal also shows typical NOESY correlation with the H33 proton signal at 3.41 ppm (Fig. S14c†). The assignment of the peak at 8.49 ppm was unsuccessful at this stage as this signal in CD_3CN showed remarkable reduction in intensity at 273 K (Fig. 5d and Fig. S17e†). We believe that the signal at 8.49 ppm originates from H12 proton of the other conformer, which is in dynamic equilibrium at RT.

In order to gain further insight into the dynamic equilibrium between two proposed conformers of **1**, temperature dependent ^{1}H NMR spectroscopy in CD_3CN was carried out. The observed changes in intensity of the H12 signal at 7.81 and 8.49 ppm as a function of temperature (Fig. S17†) was used to track the thermal equilibrium of $\mathbf{1}_{syn} \rightarrow \mathbf{1}_{anti}$ conversion. The equilibrium ratio calculated from peak integration of each of the conformers was 90:10 (syn/anti) at 273 K, which decreases gradually with increase of temperature. At 283 K, this ratio becomes 56:44 (syn/anti). No significant change in equilibrium ratio was observed after 283 K and bellow 273 K. Free energy change associated with this process (syn/anti) was calculated[62] to be $\Delta G^{\#}$ = 1.6 kcal.mol^{-1} at RT (Fig. S18†), which closely matches with computational results ($\Delta G^{\#}$ = 0.69 kcal.mol^{-1}). Hence, we conclude that presence of a dynamic equilibrium between two conformers gives rise to two different kind of hydroxyl groups (due to dissimilar hydrogen bonding) that have disparate chemical shift values. Interestingly, when the ^{1}H NMR spectrum of compound **2** in CD_3CN (Fig. 5e and Fig. S10†) was compared with that in $CDCl_3$ (Fig. S8†), we observed evidence of only a single species. This result is in stark contrast with the behaviour of compound **1** in similar environment, confirming the presence of conformational heterogeneity that originates due to the –OH appendage on molecular backbone. Finally, from our detailed NMR study we conclude that a carefully positioned –OH group in the phenyl attached to C1 atom of the imidazolyl ring is responsible for such intriguing conformational distribution in the ground state of compound **1**.

Computational Calculation

The initial ground state (S_0) and first singlet excited state (S_1) geometry of **1**, **2** and **3** were optimized using density functional theory (DFT for S_0) and time-dependent density functional theory (TDDFT for S_1).[63] Vertical excitation energies at ground state geometries were calculated using TDDFT with different functional (B3LYP, CAM-B3LYP, M06-2X).[64-69] All calculations have been enumerated using 6-311G(d,p) basis set. DFT and TDDFT calculations were carried out using GAUSSIAN09, Revision D.01 package.[70] First, using self-consistent reaction field method (SCRF)[71,72] model, we have been able to optimize ground state (S_0) geometry of **1** in ethanol (Fig. 6). Optimized geometry of S_0 state shows that the phenyl and coumarin groups attached to C3 and N2 atoms of imidazolyl ring further deviates from crystal geometry (Fig. 6). However, calculated torsional angle (0.13^o) viewed along N1–C1–C4–C5 atoms indicate that hydoxyphenyl group attached to C1 atom of imidazolyl ring is almost planar. Calculated intramolecular H-bond (O3–H•••N1, 1.65 Å, 148.62^o) (Table S3†) and presence of a pseudo-six membered aromatic ring contributes to the planarity of hydroxyphenyl group with imidazolyl ring. Rotation around the C1–C4 single bond is very promising as per as rotational isomerization is concerned. For that, a potential energy surface (PES) scan analysis has been carried out, which is used for relaxed optimizations in the ground electronic state (S_0) along with fixing the N1–C1–C4–C5 torsion in a series of values (0 to 360^o), which yielded to two different rotational conformers with 6.12 kcal.mol^{-1} potential energy barrier (Fig. 7). Moreover, calculated torsions (Table S3†) suggest that a structural rearrangement occurs upon rotation of C1–C4 single bond. Interestingly, a new putative intramolecular hydrogen bond (O3–H•••O1, 1.84 Å, 153.4^o) between O1 atom of keto carbonyl and OH proton is perceived in $\mathbf{1}_{anti}$ isomer, which is shorter in distance compared to the H-bond (O3–H•••N1, 1.890(1) Å, 148.06(0)°) obtained in single crystal (Fig. 1, and Table S3†). Our calculation also predicted that $\mathbf{1}_{syn}$ has significantly lower rotational barrier[73] (6.12 kcal.mol^{-1}) along

View Article Online
DOI: 10.1039/C7CP07274K

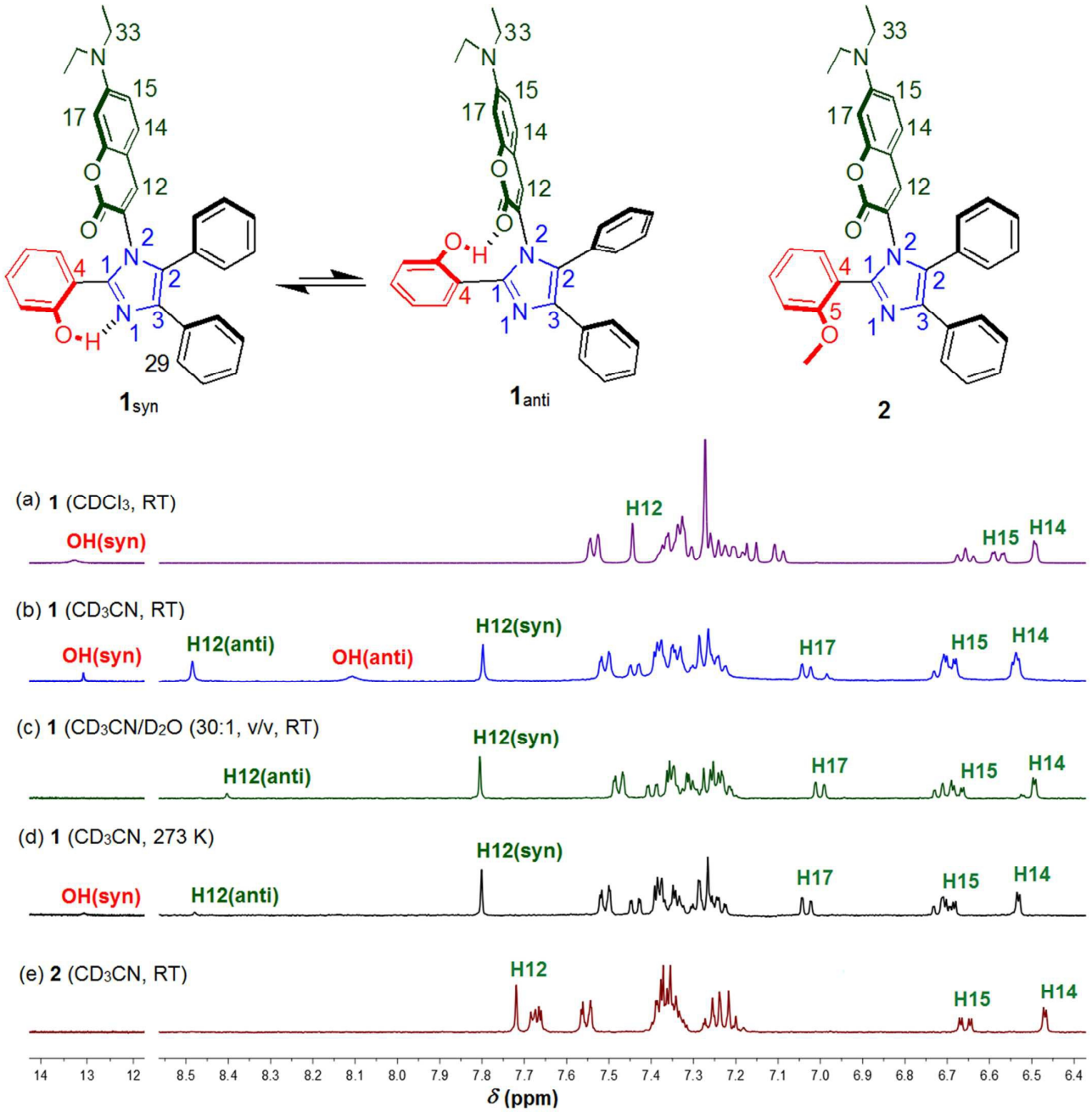

Fig. 5 ^{1}HNMR spectra (400 MHz) of **1** (a) in $CDCl_3$; (b) partial peak assignments in CD_3CN; (c) CD_3CN/D_2O (30:1), recorded after measuring in CD_3CN; (d) CD_3CN at 273 K; and (e) ^{1}HNMR spectra (400 MHz) of **2** in CD_3CN.

with low Gibbs free energy change ($\Delta G^{\#}$ = 0.69 kcal.mol^{-1}) due to formation of a new stabilizing intramolecular O–H•••O hydrogen bond upon rotation around the C1–C4 single bond. This strong intramolecular H-bond manifests itself by the formation of two conformers which were detected in ^{1}H NMR of **1** in CD_3CN. This result is consistent with NMR analysis. The final observation in support of the proposed rotation mechanism around the C1–C4 single bond was based on formation of a new stabilizing O–H•••O hydrogen bonds in $\mathbf{1}_{anti}$ isomer, which lowers their rotational barriers. In table S4, we have shown NBO[74] (B3LYP/6-311G(d,p)) interactions, which may lead to activate the rotation process around the C1–C4 bond.

View Article Online
DOI: 10.1039/C7CP07274K

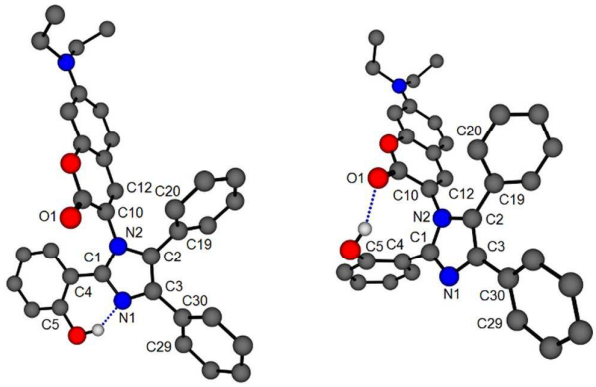

Fig. 6 Optimized geometry of $\mathbf{1}_{syn}$ and $\mathbf{1}_{anti}$. All H atoms except OH are removed for clarity.

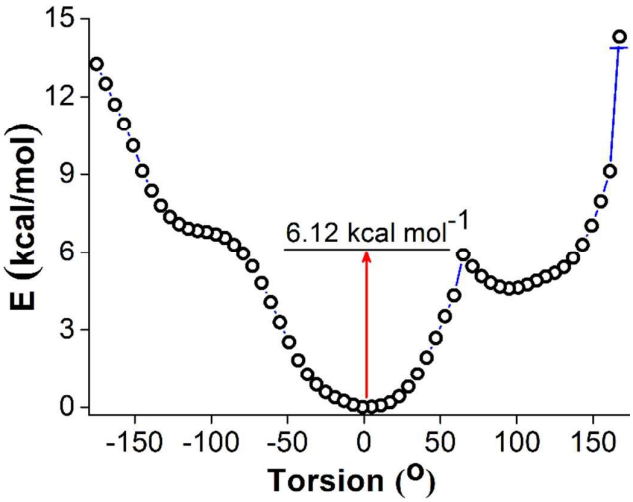

Fig. 7 Optimized potential energy surface scan when viewed along the dihedral angle [N–C1–C4–C5] of **1**.

TD-DFT calculations were used to access frontier molecular orbitals, excitation energy, and oscillator strength (*f*) for significant vertical transitions of two conformers (syn/anti). All calculated excitation energy and oscillator strength are compared in Fig. 8, Fig. S27† and Tables S5-S8†. The excitation energy of $\mathbf{1}_{syn}$ and $\mathbf{1}_{anti}$ were 3.9 eV (318 nm), 3.22 eV (385 nm), 3.01 eV (411 nm), and 3.1 eV (400 nm) respectively, which closely match with the broad absorption spectra of **1** in polar solvents (Fig. 2). These excitations should be undoubtedly assigned to the ICT transitions as judged by electron density perturbations between HOMOs and LUMOs. Interestingly, this results indicate that three electronic transitions from highest occupied molecular orbitals (HOMO) delocalized over the imidazole core along with hydroxyphenyl group attached to the C1 atom of imidazolyl ring and coumarin (HOMO-1) moieties to the lowest unoccupied molecular orbitals (LUMO and LUMO+1) delocalized over coumarin and imidazole core along with phenyl groups attached to C1 and C3 atom of imidazolyl ring (HOMO → LUMO, *f* =0.12; HOMO-1 → LUMO, *f* = 0.76; and HOMO → LUMO+1, *f* = 0.70) make major contributions to the excited states (Fig. 7). However, only one

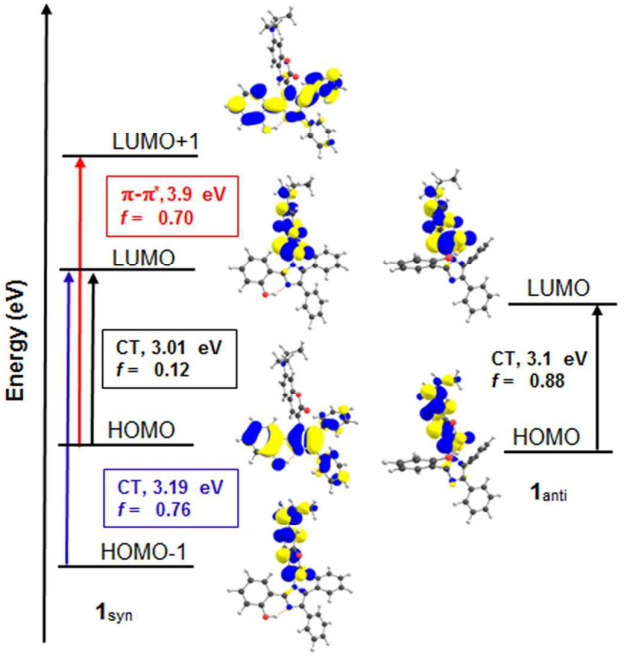

Fig. 8 Calculated molecular orbital energy levels, transition energies and oscillator strengths of the π-π* and CT transitions of the syn/anti conformers of **1**.

major electronic transition from HOMO to LUMO (HOMO→ LUMO, *f* = 0.88) was observed for $\mathbf{1}_{anti}$ conformer. For $\mathbf{1}_{anti}$, it is important to note that corresponding HOMO and LUMO is predominantly delocalized over coumarin. The calculated energy of the LUMO in $\mathbf{1}_{anti}$ conformer is lower compared to the $\mathbf{1}_{syn}$, which would explain significant stabilization of $\mathbf{1}_{anti}$ conformer in the excited state due to distal intramolecular H-bond between OH proton and O1 atom of keto carbonyl from coumarin segment. The corresponding contour surface (Fig. S27†) and excitation energy of **2** and **3** shows almost similar results (Table S7 and S8†).

Computational results further suggests that a significant orbital re-distribution is observed between two conformers, indicating structural re-adjustment caused by distal intramolecular H-bonds. Bassed on an extensive study of NMR, X-ray data, ultrafast spectroscopy measurements, and computations using density functional theory (DFT) at the B3LYP/6-311G(d,p), an overall scenario for solvent induced rotamerization of **1** is summerised in Fig. 9.

Conclusions

In summary, we successfully demonstrate a novel design principle for tuning lifetime of a coumarin fluorophore which is conjugated to tri-phenyl-imidazole moiety, **1**, by introducing an –OH group on the imidazolyl fragment remote to the dye. Although the –OH functionality renders two ground state conformers of **1** as confirmed by ^{1}H-NMR, we attribute fluorescence lifetime change to the establishment of a putative O–H•••O interaction subsequent to local photoexcitation at the coumarin. Spectroscopic measurements tracking the excited state dynamics provide unequivocal

View Article Online
DOI: 10.1039/C7CP07274K

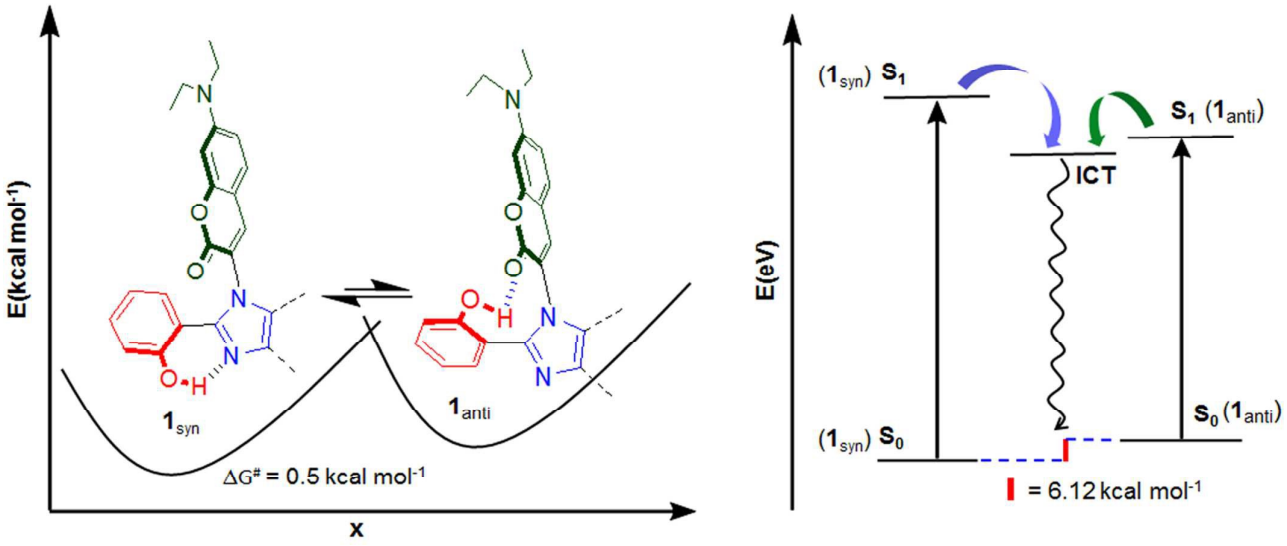

Fig. 9 Model for the ground state and excited state behaviour of **1**.

evidence for bond rotation, which was affected by solvent viscosity. Although the barrier for ground state rotation is 6.12 Kcal/mol in **1**, photoexcitation of coumarin leads to facile rotation along the C1–C4 bond leading to the formation of long-lived *anti* state. Systematic measurements on two other coumarin-imidazole conjugates **2** and **3**, showed *ca*. 4-5 times reduction in the emission lifetimes thereby supporting our design principle. The novelty of our work therefore lies in highlighting the role of a distal functionality in tweaking the fate of localized coumarin emission. In principle, our work provides a new scheme to implement conformational control on the photophysics of molecular fluorophores, and should inspire novel framework to control function through rational design of chemical interactions.

Experimental Section

Materials and Reagents

7-N,N-diethylaminosalicyaldehyde and ethyl nitroacetate were purchased from Alfa aesar and rest all chemicals were purchased from local source. All deuterated solvents were purchased from Euroisotope. Thin-layer chromatography (TLC) analyses were carried out on pre-coated silica gel plates (Merck) and spots were visualized by UV irradiation. Column chromatography was performed on glass columns loaded with silica gel. All spectroscopic measurement had been accomplished by using freshly distilled solvent.

Physical measurements and Instrumentation

Liquid state NMR were recorded in Bruker AVHDN 400 with working frequencies of 400.245 MHz for ^{1}H nuclei and 100.6419 MHz for ^{13}C nuclei, respectively, using $CDCl_3$, CD_3CN and D_2O as solvent. Chemical shifts were quoted in ppm relative to tetramethylsilane, using residual solvent peak as a reference standard. High Resolution Mass Spectroscopy (HRMS) were carried out using an Agilent 6540 accurate–mass Q-TOF LC/MS (Agilent Technologies, U.S.A.). MALDI-TOF mass spectra were obtained on a Bruker UltrafleXtreme(TM) (Bruker Daltonics). Samples in buffer (0.5 μL) were mixed with a solution of 3,5-Dimethoxy-4-hydroxycinnamic acid (1:1 MeCN:H_2O with 0.1% trifluoroacetic acid, 0.5 μL) and applied on the MALDI plate. Samples were allowed to dry completely before analysis. Infrared spectroscopy had been implemented by using Thermo Fisher scientific FTIR. Steady state absorbance were measured by Agilent Technologies Cary 8454 UV/vis instrument. Steady-state emission was recorded in fluorescence spectrometer (Model: FL3-2-IHR from Horiba) with standard FL3 PMT R928P detector were used for steady state emission. Fluorescence quantum yields in each case were determined by comparing the corrected spectrum with standard Fluorescin[22] (ϕ = 0.85 in 0.1(N) NaOH taking area under the total emission.

Nano-second lifetimes were measured using fluorescence intensity decay of a TCSPC set up, coupled with a pico-second laser. The excitation source was frequency doubled output of a mode-locked picosecond Ti-sapphire laser (Tsunami, Spectra-Physics, USA) (720-900 nm) pumped by a diode pumped CW Nd-vanadate laser (532 nm) (Millennia X, Spectra-Physics, USA). The pulse width of the exciting laser was typically 1-2 ps with repetition rate of 80 MHz. Fluorescence decay curves were obtained using a microchannel plate photomultiplier (model R2809; Hamamatsu Corp.) coupled with a time-correlated single photon-counting setup. The instrument response functions (IRF) at 400 nm were obtained by collecting scattering using a dilute colloidal suspension of dried non-dairy coffee whitener. The width (fwhm) of the instrument response function (IRF) was ~100 ps. The decay kinetics were fitted with multi-exponential by iterative method using IGOR Pro 5.01 software.

Upconversion measurements[23] for all samples were performed in a rotating sample chamber of 1 mm path length, were excited using the second harmonic (398 nm) of a mode-locked

View Article Online
DOI: 10.1039/C7CP07274K

Ti-sapphire laser (Tsunami, Spectra Physics, average power 1W at 800 nm, pulse width 200 fs, repetition rate 80 MHz) pumped with a CW 5 W Millennia (Spectra Physics) DPSS laser. The fluorescence emitted from the samples was upconverted in a nonlinear crystal by mixing with a gate pulse, which consists of a portion of the fundamental beam. The upconverted light was dispersed in a monochromator and detected by photon counting electronics. The femtosecond fluorescence kinetics were fitted using a Gaussian function of 250 fs FWHM of the IRF for the excitation pulse using IGOR Pro 5.01 software.

Synthesis and Characterization

General procedures for compounds **1**, **2** and **3**. These compounds were synthesized using a modified multi component cyclisation reaction.[15] In a 25 ml round-bottomed flask, compound **1b** (250 mg, 1.0 equiv.), substituted benzaldehyde (1.0 equiv.) (salicylaldehyde for **1**; 2-methoxybenzaldehyde for **2**; and benzaldehyde for **3**), benzil (1.0 equiv.) and ammonium acetate (6.0 equiv.) were taken in 10 mL acetic acid and then allowed to reflux for 18 h. After completion, reaction mixture was poured into ice water, precipitate was filtered out and dissolved in ethyl acetate. The crude was purified by column chromatography using silica 100-200 mesh and ethyl acetate/hexane mixture as eluent.

*7-(diethylamino)-3-(2-(2-hydroxyphenyl)-4,5-diphenyl-1H-imidazol-1-yl)-2H-chromen-2-one (**1**)*. Yellow crystals. Yield: 0.72 g (68 %). ^{1}H NMR (400 MHz, $CDCl_3$, δ/ppm): δ 13.29 (bs, 1H), 7.53 (d, 2H), 7.43 (s, 1H), 7.31-7.36 (m, 6H), 7.25-7.14 (m, 4H), 7.10 (s, 1H), 6.64 (t, 1H), 6.55 (d, 1H), 6.48 (s, 1H), 3.40 (q, 4H), 1.20 (t, 6H) ppm. ^{1}H NMR (400 MHz, CD_3CN, δ/ppm): 13.10 (bs, 1H), 7.83 (s, 1H), 7.55-7.52 (m, 3H), 7.42-7.32 (m, 6H), 7.29-7.27 (m, 3H), 7.07 (d, J = 8 Hz, 1H), 6.76-6.71 (m, 2H), 6.56 (s, 1H), 3.48 (q, J = 8 Hz, 4H), 1.19 (t, J = 8Hz, 6H). ^{13}C NMR (100 MHz, $CDCl_3$, δ/ppm): δ 159.68, 156.55, 151.58, 148.25, 143.02, 138.35, 134.49, 131.69, 131.01, 130.79, 130.76, 129.75, 128.79, 128.57, 128.52, 128.21, 127.37, 126.65, 117.40, 109.38, 106.99, 97.29, 45.03, 12.53 ppm. IR data (solid): 3760 (O-H), 1729 (C=O) cm^{-1}. MALDI-TOF-MS, (matrix: 3,5-Dimethoxy-4-hydroxycinnamic acid): calculated for $C_{34}H_{29}N_3O_3$ 527.2209; found 527.2213 [M$^+$].

*7-(diethylamino)-3-(2-(2-methoxyphenyl)-4,5-diphenyl-1H-imidazol-1-yl)-2H-chromen-2-one (**2**)*. Yellow crystals. Yield: 0.81 g (75 %). ^{1}H NMR (400 MHz, $CDCl_3$, δ/ppm): δ 7.70 (d, 1H), 7.59 (d, 2H), 7.38 (s, 2H), 7.32-7.27 (m, 5H), 7.23-7.13 (m, 2H), 7.07-7.00 (m, 3H), 6.74 (d, 1H), 6.48 (d, Hz, 1H), 3.64 (s, 3H), 3.34 (q, 4H), 1.15 (t, 6H) ppm. ^{13}C NMR (100 MHz in $CDCl_3$): δ 156.95, 156.35, 151.2, 140.85, 138.25, 134.76, 132.87, 131.08, 130.93, 130.66, 129.33, 128.61, 128.27, 128.11, 127.50, 126.46, 121.10, 117.81, 110.92, 109.07, 107.07, 97.35, 55.28, 44.95, 12.55 ppm. IR data (solid): 1710 (C=O) cm^{-1}. HRMS(ESI): m/z calculated for $C_{35}H_{31}N_3O_3$: 541.2365, found [M-H$^+$]: $C_{35}H_{32}N_3O_3^+$, 542.2431 (calcd 542.2438).

*7-(diethylamino)-3-(2,4,5-triphenyl-1H-imidazol-1-yl)-2H-chromen-2-one (**3**)*. Yellow crystals. Yield: 0.76 g (63 %). ^{1}H NMR (400 MHz, $CDCl_3$, δ/ppm): δ 7.73 (d, 2H), 7.62 (d, 2H), 7.40-7.19 (m, 12H), 7.13 (d, 1H), 6.55 (dd, 1H), 6.43 (s, 1H), 3.43 (q, 4H), 1.22 (t, 6H) ppm. ^{13}C NMR (100 MHz, $CDCl_3$, δ/ppm): δ 155.32, 154.21, 149.89, 146.31, 143.42, 139.53, 135.11, 130.66, 131.01, 130.79, 129.92, 128.95, 128.79, 128.52, 128.43, 128.02, 126.91, 126.82, 117.40, 109.38, 107.01, 97.29, 45.03, 12.53 ppm. IR data (solid): 1715 (C=O) cm^{-1}. HRMS(ESI): m/z calculated for $C_{34}H_{29}N_3O_2$: 511.2260, found [M-H$^+$]: $C_{34}H_{30}N_3O_2^+$, 512.2328 (calcd 512.2333).

Conflicts of interest

There are no conflicts to declare.

Acknowledgements

Financial support for this work was provided by the Science & Engineering Research Board (SERB) (File No: SB/EMEQ-004/2014 & YSS/2014/000923), DST, and Shiv Nadar University (SNU), India. I. B. thanks SNU for fellowship. JD thanks TIFR and the Department of Atomic Energy (DAE) for financial support. We thank N. Sukumar for computational help.

References

1 Jeffrey, G. A. *An Introduction to Hydrogen Bonding*; Oxford University Press: USA, 1997.
2 G. J. McManus, J. J. Perry, M. Perry, B. D. Wagner and M. J. Zaworotko, *J. Am. Chem. Soc.,* 2007, **129**, 9094-9101.
3 O. A. Sytina, D. J. Heyes, C. N. Hunter, M. T. Alexandre, I. H. M. van Stokkum, R. van Grondelle and M. L. Groot, *Nature,* 2008, **456**, 1001-1005.
4 T. A. V. Khuong, J. E. Nunez, C. E. Godinez, M. A. Garcia-Garibay, *Acc. Chem. Res.,* 2006, **39**, 413-422.
5 J. Zhao, M. G. Davidson, M. F. Mahon, G. Kociok-Köhn and T. D. James, *J. Am. Chem. Soc.,* 2004, **126**, 16179-16186.
6 G.-J. Zhao and K.-L. Han, *Acc. Chem. Res*., 2012, **45**, 404-413.
7 L. M. Tolbert and K. M. Solntsev, *Acc. Chem. Res*., 2002, **35**, 19-27.
8 Y. Yamada, N. Mikami and T. Ebata, *Proc. Natl. Acad. Sci. U.S.A.,* 2008, **105**, 12690-12695.
9 A. Kawanabe, Y. Furutani, K. H. Jung and H. Hideki Kandori, *J. Am. Chem. Soc.,* 2009, **131**, 16439-16444.
10 L. Zhang, Y. Yang, Y. T. Kao, L. J. Wang and D. P. Zhong, *J. Am. Chem. Soc.* 2009, **131**, 10677-10691.
11 X. Z. Yan, J. Pawlas, T. Goodson III., and J. F. Hartwig, *J. Am. Chem. Soc.*, 2005, **127**, 9105-9116.
12 Y. Wang, G. S. He, P. N. Prasad and T. Goodson III., *J. Am. Chem. Soc.*, 2005, **127**, 10128-10129.
13 O. Tishchenko, D. G. Truhlar, A. Ceulemans and M. T. Nguyen, *J. Am. Chem. Soc.*, 2008, **130**, 7000-7010.
14 D. Sicinska, D. G. Truhlar and P. Paneth, *J. Am. Chem. Soc.*, 2005, **127**, 5414-5422.
15 K.-L. Han, G.-J. Zhao, *Hydrogen Bonding and Transfer in the Excited State*; Wiley-Blackwell, John Wiley & Sons Ltd.: Chichester PO19 8SQ, UK, 2010.
16 M. A. van der Horst, T. P. Stalcup, S. Kaledhonkar, M. Kumauchi, M. Hara, A. H. Xie, K. J. Hellingwerf and W. D. Hoff, *J. Am. Chem. Soc.*, 2009, **131**, 17443-17451.
17 G.-J. Zhao and K.-L. Han, *Acc. Chem. Res*., 2011, **45**, 404-413.
18 P.-L. Zhao, L. Wang, X.-L. Zhu, X.-Q. Huang, C.-G. Zhan, J.-W. Wu and G.-F. Yang, *J. Am. Chem.*, *Soc.* 2010, **132**, 185-194.
19 J. E. Raymond, A. Bhaskar, T. Goodson III., N. Makiuchi, K. Ogawa and Y. Kobuke, *J. Am. Chem. Soc.*, 2008, **130**, 17212-17213.

View Article Online
DOI: 10.1039/C7CP07274K

20 N. Barman, D. Singha and K. Sahu, *J. Phys. Chem.*, *A* 2013, **117**, 3945-3953.
21 N. P. Wells, M. J. McGrath, J. I. Siepmann, D. F. Underwood, D. A. Blank, *J. Phys. Chem. A,* 2008, **112**, 2511-2514..
22 B. L. Feringa, Ed. *Molecular Switches*; Wiley-VCH: Weinheim, Germany, 2001.
23 E. R. Kay, D. A. Leigh and F. Zerbetto, *Angew. Chem., Int. Ed*., 2007, **46**, 72-191.
24 B. Champin, P. Mobian and J.-P. Sauvage, *Chem. Soc. Rev*., 2007, **36**, 358-366.
25 V. Balzani, A. Credi, M. Venturi, Molecular Devices and Machines: Concepts and Perspectives for the Nanoworld; Wiley-VCH: Weinheim, Germany, 2008.
26 G. Vives, J. M. Tour, *Acc. Chem. Res*., 2009, **42**, 473-487.
27 J. F. Stoddart, *Chem. Soc. Rev*., 2009, **38**, 1802-1820.
28 P. C. Knipe, S. Thompson and A. D. Hamilton, *Chem. Sci*., 2015, **6**, 1630-1639.
29 R. Klajn, *Chem. Soc. Rev*., 2014, **43**, 148-184.
30 X. Su, S. Voskian, R. P. Hughes and I. Aprahamian, *Angew. Chem*. Int. Ed., 2013, **52**, 10734-10939.
31 K. Miwa, Y. Furusho and E. Yashima, *Nat. Chem*., 2010, **2**, 444-449.
32 P. Amrhein, A. Shivanyuk, D. W. Johnson and J. Rebek, *J. Am. Chem. Soc*., 2002, **124**, 10349-10358.
33 S. Akine, S. Hotate and T. Nabeshima, *J. Am. Chem. Soc*., 2011, **133**, 13868; (d) G. Haberhauer, *Angew. Chem., Int. Ed*., 2008, **47**, 3635-13871.
34 F. Durola and J. Rebek, *Angew. Chem., Int. Ed*., 2010, **49**, 3189-3191.
35 J. Bergueiro, F. Freire, E. P. Wendler, J. M. Seco, E. Quinóa and R. Riguera, *Chem. Sci*., 2014, **5**, 2170-2176.
36 X. Yang, L. Yuan, K. Yamato, A. L. Brown, W. Feng, M. Furukawa, X. C. Zeng and B. Gong, *J. Am. Chem. Soc*., 2004, **126**, 3148-3162.
37 I. M. Jones and A. D. Hamilton, Org. Lett., 2010, **12**, 3651-3653.
38 P. C. Knipe, I. M. Jones, S. Thompson and A. D. Hamilton, *Org. Biomol. Chem*., 2014, **12**, 9384-9388.
39 T.-Z. Xie, C. Guo, S.-Y. Yu and Y.-J. Pan, *Angew. Chem., Int. Ed*., 2012, **51**, 1177-1181.
40 C. R. Jones, P. K. Baruah, A. L. Thompson, S. Scheiner and M. D. Smith, *J. Am. Chem. Soc*., 2012, **134**, 12064-5424.
41 S. Toyota, *Chem. Rev*., 2010, **110**, 5398-5424.
42 J.-M. Suk, V. R. Naidu, X. Liu, M. S. Lah and K.-S. Jeong, *J. Am. Chem. Soc*., 2011, **133**, 13938-13941.
43 R. M. Meudtner and S. Hecht, *Angew. Chem., Int. Ed*., 2008, **47**, 4926-4930.
44 A. Brenlla, F. Rodríguez-Prieto, M. Mosquera, M. A. Ríos and M. C. R. Rodríguez, *J. Phys. Chem*. A, 2009, **113**, 56-67.
45 D. Ray and P. K. Bharadwaj, *Inorg. Chem*., 2008, **47**, 2252.
46 S. Park, O.-W. Kwon, S. Kim, S. Park, M.-G. Choi, M. Cha, S.-Y. Park and D. J. Jang, *J. Am. Chem. Soc*., 2005, **127**, 10070.
47 Various attempts to grow single crystals of reference compound, **2** were unsuccessful.
48 S. Park, O.-H. Kwon, S.-H. Kim, J. Seo, K. Chung, S.-Y. Park, D.-J. Jang, B. M. Medina, J. Gierschner and S.-Y. Park, *J. Am. Chem. Soc*., 2009, **131**, 14043-14049.
49 S. Park, O.-H. Kwon, Y.-H. Lee, D.-J. Jang and S. Y. Park, *J. Phys. Chem*. A, 2007, **111**, 9649-9653.
50 S. Park, O.-H. Kwon, S. Kim, S. Park, M.-G. Choi, M. Cha, S. Y. Park and D.-J. Jang, *J. Am. Chem. Soc.*, 2005, **127**, 10070-10074.
51 N. C. Lim and C. Brückner, *Chem. Commun*., 2004, 1094.
52 *Molecular Fluorescence: Principles and applications*, B. Valeur, M. N. Berberan-Santos, Ed. Wiley-VCH: Verlag GmbH, 2001.
53 S. R. Trenor, A. R. Shultz, B. J. Love and T. E. Long, *Chem. Rev*., 2004, **104**, 3059-3078.
54 N. C. Lim, J. V. Schuster, M. C. Porto, M. A. Tanudra, L. Yao, H. C. Freake, C. Brückner, *Inorg. Chem*., 2005, **44**, 2018-2030.
55 X. Liu, J. M. Cole, P. G. Waddell, T.-C. Lin, J. Radia and A. Zeidler, *J. Phys. Chem*. A, 2012, **116**, 727-737.
56 X. Liu, J. M. Cole, P. G. Waddell, T.-C. Lin and S. McKechnie, *J. Phys. Chem.* C, 2013, **117**, 14130-14141.
57 G. Jones II, W. R. Jackson, C.-Y.Choi and W. R. Bergmark, *J. Phys. Chem*., 1985*,* **89***,* 294.
58 T. Eckardt, V. Hagen, B. Schade, R. Schmidt, C. Schweitzer and J. Bendig, *J. Org. Chem. Soc*., 2002, **67**, 703.
59 C. A. Paeker and W. T. Ress, *Analyst*. 1960, **85**, 587-600.
60 T. Gabe, Y. Urano, K. Kikuchi, H. Kojima and T. Ngano, *J. Am. Chem. Soc*. 2004, **126**, 3357-3367.
61 S. Chatterjee, P. Karuso, A. Boulangé, P. A. Peixoto, X. Franck and A. Datta, *J. Phys. Chem*. B 2013, **117**, 14951-14959.
62 We could not extend the rate constant measurement studies in CD_3CN because of low free energy of activation energy ($\Delta G^{\#}$ = - 0.1 kcal mol^{-1}) at 283 K. In order to reach a better conclusion about the mechanism, one has to look at the full analysis of NMR.
63 E. Runge and E. K. U. Gross, *Phys. Rev. Lett*. 1984, **52**, 997.
64 A. D. Becke, *J. Chem. Phys*., 1993, **98**, 5648-5652.
65 C. Lee, W. Yang and R. G. Parr, *Phys. Rev.* B, 1988, **37**, 785-789.
66 S. H. Vosko, L. Wilk and M. Nusair, *Can. J. Phys*. 1980, **58**, 1200-1211.
67 P. J. Stephens, F. J. Devlin, C. F. Chabalowski and M. J. Frisch, *J. Phys. Chem*., 1994, **98**, 11623-11627.
68 Y. Takeshi, P. T. David and C. H. Nicholas *Chem. Phys. Lett*., 2004, **393**, 51-57.
69 Y. Zhao and D. G. Truhlar, *Theor. Chem. Acc*., 2008, **120**, 215-241.
70 M. J. Frisch, G. W. Trucks, H. B. Schlegel, G. E. Scuseria, M. A. Robb, J. R. Cheeseman, G. Scalmani, V. Barone, B. Mennucci, G. A. Petersson, H. Nakatsuji, M. Caricato, X. Li, H. P. Hratchian, A. F. Izmaylov, J. Bloino, G. Zheng, J. L. Sonnenberg, M. Hada, M. Ehara, K. Toyota, R. Fukuda, J. Hasegawa, M. Ishida, T. Nakajima, Y. Honda, O. Kitao, H. Nakai, T. Vreven, J. A. Montgomery Jr., J. E. Peralta, F. Ogliaro, M. Bearpark, J. J. Heyd, E. Brothers, K. N. Kudin, V. N. Staroverov, T. Keith, R. Kobayashi, J. Normand, K. Raghavachari, A. Rendell, J. C. Burant, S. S. Iyengar, J. Tomasi, M. Cossi, N. Rega, J. M. Millam, M. Klene, J. E. Knox, J. B. Cross, V. Bakken, C. Adamo, J. Jaramillo, R. Gomperts, R. E. Stratmann, O. Yazyev, A. J. Austin, R. Cammi, C. Pomelli, J. W. Ochterski, R. L. Martin, K. Morokuma, V. G. Zakrzewski, G. A. Voth, P. Salvador, J. J. Dannenberg, S. Dapprich, A. D. Daniels, O. Farkas, J. B. Foresman, J. V. Ortiz, J. Cioslowski and D. J. Fox, Gaussian, Inc., Wallingford CT, 2013.
71 M. W. Wong, M. J. Frisch and K. B. Wiberg, *J. Am. Chem. Soc*., 1991, **113**, 4776-4782.
72 M. W. Wong, K. B. Wiberg and M. J. Frisch, *J. Am. Chem. Soc*., 1992, **114**, 523-529.
73 B. E. Dial, P. J. Pellechia, M. D. Smith and K. D. Shimizu, *J. Am. Chem. Soc.*, 2012, **134**, 3675.
74 A. E. Reed and F. Weinhold, *J. Chem. Phys*. 1983, **78**, 4066-4073.

View Article Online
DOI: 10.1039/C7CP07274K

Table of Contents

Conformational switching via intramolecular H-bond modulates fluorescence lifetime in a novel coumarin-imidazole conjugate